Inorganic Chemistry

Article

pubs.acs.org/IC

Pressure-Induced Local Lattice Distortions in α-$Co[N(CN)_2]_2$

J. L. Musfeldt,*[,†] T. V. Brinzari,[†] J. A. Schlueter,[‡] J. L. Manson,[§] A. P. Litvinchuk,[⊥] and Z. Liu[∥]

[†]Department of Chemistry, University of Tennessee, Knoxville, Tennessee 37996, United States

[‡]Materials Science Division, Argonne National Laboratory, Argonne, Illinois 60439, United States

[§]Department of Chemistry, and Biochemistry, Eastern Washington University, Cheney, Washington 99004, United States

[⊥]Texas Center for Superconductivity and the Department of Physics, University of Houston, Houston, Texas 77204, United States

[∥]Geophysical Laboratory, Carnegie Institution of Washington, Washington, DC 20015, United States

ABSTRACT: This work brings together diamond anvil cell techniques, vibrational spectroscopies, and complementary lattice dynamics calculations to investigate pressure-induced local lattice distortions in α-$Co[N(CN)_2]_2$. Analysis of mode behavior and displacement patterns reveals a series of pressure-driven transitions that modify the CoN_6 counter-rotations, distort the octahedra, and flatten the C—N_{ax}—C linkages. These local lattice distortions may be responsible for the low temperature magnetic crossover. We also discuss prospects for negative thermal expansion and show that there is not a straightforward low pressure pathway between the pink α and blue β ambient pressure phases of $Co[N(CN)_2]_2$.

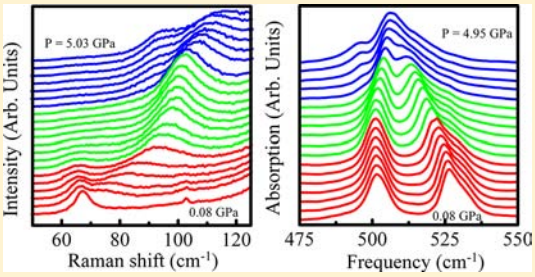

INTRODUCTION

The interplay between structure and magnetism underpins a variety of properties in functional materials.[1,2] Spin−lattice interactions stabilize the development of many interesting ground states, for instance spin Peierls,[3−5] multiferroic,[6,7] and the fully polarized state that results from a magnetic quantum critical transition.[8,9] Magnetostructural correlations are traditionally developed using a combination of bulk magnetic and structural probes like susceptibility and X-ray diffraction,[10,11] magnetostriction measurements,[12−14] and vibrational spectroscopies.[5,15−17] $Co[N(CN)_2]_2$ ($[N(CN)_2]^-$ = dicyanamide) attracted our attention as a system where the bulk aspects of magnetoelastic coupling have received sustained attention,[18−21] but where the microscopic signatures of this coupling are wholly unexplored. The simple chemical structure and soft, flexible framework are also well-suited for our investigations. α-$Co[N(CN)_2]_2$ is a magnetic insulator that crystallizes in a three-dimensional distorted rutilelike structure (space group *Pnnm*) and is a member of an isostructural family of compounds with general formula $M^{II}[N(CN_2)]_2$ (M = Mn, Fe, Co, Ni, Cu).[18−23] The Co^{2+} ion resides at the center of an axially elongated octahedron with dicyanamide ligands coordinated via nitrile nitrogens in the equatorial plane and via amide nitrogens in the axial direction. It is a collinear ferromagnet below T_C = 9 K with well-defined hysteresis loops and spin orientation along the *c*-axis.[18,19,21] The dominant superexchange ($J \approx 4$ K) proceeds through the Co—N≡C—N—Co path.[24] The pink ambient pressure compound is traditionally called α-$Co[N(CN)_2]_2$. There is also a blue ambient pressure β-phase material.[18] A blue form also presents itself under pressure (for instance, around the edges of a KBr pellet when pressure is released).[25] It is not known whether the blue β-phase obtained by chemical methods is similar to the short-lived blue material that appears under pellet-making conditions. A structural transition labeled $\alpha \rightarrow \gamma$ is also thought to take place near 1 GPa,[26] although at this time, it is not known how the pressure-induced γ-phase arises or how the lattice dynamics compare to the more well-studied α-morphology. Pressure drives not only an orthorhombic → (probably) monoclinic structural transition[26] but also a concomitant crossover from the ferromagnetic → antiferromagnetic state near 1 GPa.[20] We can understand this finding in a general sense by recalling that pressure directly modifies bond lengths and bond angles and that changes in the local structure impact the magnetic properties.[27]

To investigate the microscopic aspects of magnetoelastic coupling in α-$Co[N(CN)_2]_2$, we measured the vibrational response as a function of pressure and compared our findings with complementary lattice dynamics calculations. Our combined infrared and Raman spectra unexpectedly reveal that this system has multiple transitions. There is a major change in the lattice at 1 GPa that we assign as the $\alpha \rightarrow \gamma$ structural transition. Here, compression modifies the CoN_6 counter-rotation, distorts the octahedra by accentuating the axial elongation and breaking symmetry in the plane, and flattens the C—N_{ax}—C linkages. Although the exact connection of these local lattice distortions to the magnetic crossover is still to be uncovered, the similar pressure scale suggests that they may be related. We also discover an additional $\gamma \rightarrow \delta$ transition near 3 GPa that takes place within the context of a relatively similar space group, relieving the

Received: August 4, 2013
Published: December 3, 2013

   dx.doi.org/10.1021/ic402010h | *Inorg. Chem.* 2013, 52, 14148−14154

degeneracy of octahedral rotation about the C_4 symmetry axes and spliting local modes. Finally, we weigh in on prospects for negative thermal expansion and use a comparison of our high pressure spectra of $Co[N(CN)_2]_2$ with measurements of the blue as-synthesized β-phase material to show that the local structures are quite different.

MATERIALS AND METHODS

Pink polycrystalline α-$Co[N(CN)_2]_2$ was prepared as described previously[18] and loaded into a symmetric diamond anvil cell either neat or with a pressure medium (vacuum grease or KBr) and a ruby ball. Ruby fluorescence was used to determine pressure, and the pressure medium served to minimize nonhydrostatic effects.[28] Our variable pressure infrared and Raman scattering (λ_{exc} = 532 nm, 1.2 mW) measurements employed the U2A beamline facilities at the National Synchrotron Light Source, Brookhaven National Laboratory. The high brightness synchrotron source is particularly important for overcoming throughput limitations imposed by the 500 μm diamond culets, the 180 μm gasket, and far-infrared diffraction effects.[29] The spectral resolution was between 1 and 2 cm^{-1}, depending on the experiment, and compression was reversible, with no hysteresis within our sensitivity. Standard fitting techniques were employed to follow peak position vs pressure trends. The blue as-synthesized β-$Co[N(CN)_2]_2$ was measured at ambient pressure for comparison. Density functional calculations were performed on the isostructural $Mn[N(CN)_2]_2$ analog within the generalized-gradient approximation using revised Perdew–Burke–Ernzerhof[30] functionals as implemented in the CASTEP code[31] along with norm-conserving pseudopotentials. Integration over the Brillouin zone was performed over the 2 × 2 × 2 Monkhorst–Pack grid in reciprocal space.[32] The lattice vibrations were calculated using the linear response method.[33]

RESULTS AND DISCUSSION

Lattice Dynamics as a Probe of Symmetry and Phase Transition Mechanisms. Vibrational spectroscopies are sensitive, microscopic techniques, well-suited for revealing magnetoelastic interactions and local lattice distortions. Common signatures of phase boundaries include the appearance (or disappearance) of new features, changes in the mode splitting pattern, and frequency shifts.[5,16,34] A factor group analysis[35] for the *Pnnm* space group yields 25 infrared active modes $\Gamma_{infrared} = 7B_{1u} + 9B_{2u} + 9B_{3u}$ and 30 Raman active vibrations $\Gamma_{Raman} = 8A_g + 8B_{1g} + 7B_{2g} + 7B_{3g}$. Figure 1 displays the complete infrared and Raman spectra of α-$Co[N(CN)_2]_2$ at room temperature. We assign the spectral features using our previously reported mode frequencies, symmetries, and displacement patterns for isostructural $Mn[N(CN)_2]_2$.[9,36] The low frequency modes are especially interesting under compression.

Infrared Vibrational Spectroscopy Revealing Multiple Pressure-Induced Transitions. The infrared spectrum of α-$Co[N(CN)_2]_2$ displays a rich vibrational pattern, in line with what we expect from the symmetry analysis.[36] Figure 2a,d,g shows close-up views of three representative mode clusters. The frequency vs pressure trends are presented in Figure 2b,e,h, and schematic diagrams of three representative displacement patterns are shown in Figure 2c,f,i. It is easy to identify critical pressures at 1 and 3 GPa from the mode splittings and inflection points in the frequency vs pressure data. The infrared response is more sensitive than the Raman spectra in this regard. We therefore rely primarily on the data in Figure 2 to determine the critical pressures of α-$Co[N(CN)_2]_2$ and to identify the three phases that we label as α, γ, and δ. The critical pressures are modest because $Co[N(CN)_2]_2$ is a flexible molecular material with relatively low energy scales.

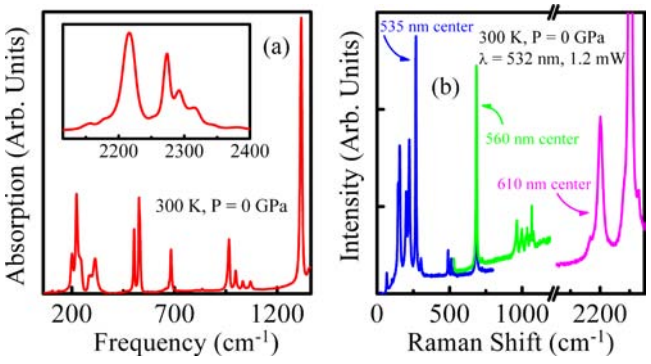

Figure 1. (a) Complete infrared spectrum of α-$Co[N(CN)_2]_2$ at 300 K. (b) Complete Raman spectrum of α-$Co[N(CN)_2]_2$ at 300 K. The background levels differ due to different integration times.

The infrared response of α-$Co[N(CN)_2]_2$ reveals 1 → 2 splitting of several low frequency modes at 1 GPa.[37] Importantly, the two Co^{2+} displacement modes at ≈105 and 135 cm^{-1} split (as does the 177 cm^{-1} feature), indicative of two unique Co^{2+} environments and a more complicated unit cell in the γ-phase. Although pressure compresses the CoN_6 octahedra overall, it accentuates the axial distortion that already exists at ambient conditions.[38] From a chemical point of view, the relative octahedral elongation above 1 GPa occurs because the nitrile nitrogens in the equatorial plane ligands are more compressible than the amide nitrogens in the axial direction. Evidence for this overall distortion comes from splitting of the combined Co—N_{ax} and Co—N_{eq} stretching mode at 289 cm^{-1} in which the axial component is more relaxed and therefore forms the lower frequency branch (Figure 2b). This modification makes α-$Co[N(CN)_2]_2$ more like the antiferromagnetic Mn analog in terms of the relative elongation of the octahedra.[38] Pressure influences the in-plane geometry as well. Splitting of the low frequency Co^{2+} displacement modes (which have a shearing pattern) as well as the low frequency wagging modes suggests an in-plane tetragonal distortion under pressure. Thus, in addition to a disproportionately elongated octahedron, the CoN_6 building block units break symmetry in the equatorial plane. The softer branch of each doublet above 1 GPa supports this supposition. The spectra also display several clusters with both peak coalescence and splitting depending on the pressure. The cluster near 500 cm^{-1} is a good example of this behavior (Figure 2g). With increasing pressure, the out-of-plane symmetric N—C—N bend collapses into the in-plane asymmetric N—C—N bend, and another peak emerges at 495 cm^{-1} when the $\gamma \rightarrow \delta$ transition is complete. Finally, the infrared-active branches of the in-plane symmetric C—N_{ax}—C bending and C—N symmetric stretching modes at 683 and 966 cm^{-1} display strong pressure-induced red shifts in the 0–5 GPa regime. This behavior is consistent with the Raman response discussed below and supports the finding of flexible (and flatter) superexchange ligands under compression.

Taken together, our infrared work reveals two structural transitions. The $\alpha \rightarrow \gamma$ transition at 1 GPa takes place with a major crystallographic change to a cell with lower crystal

dx.doi.org/10.1021/ic402010h | Inorg. Chem. 2013, 52, 14148–14154

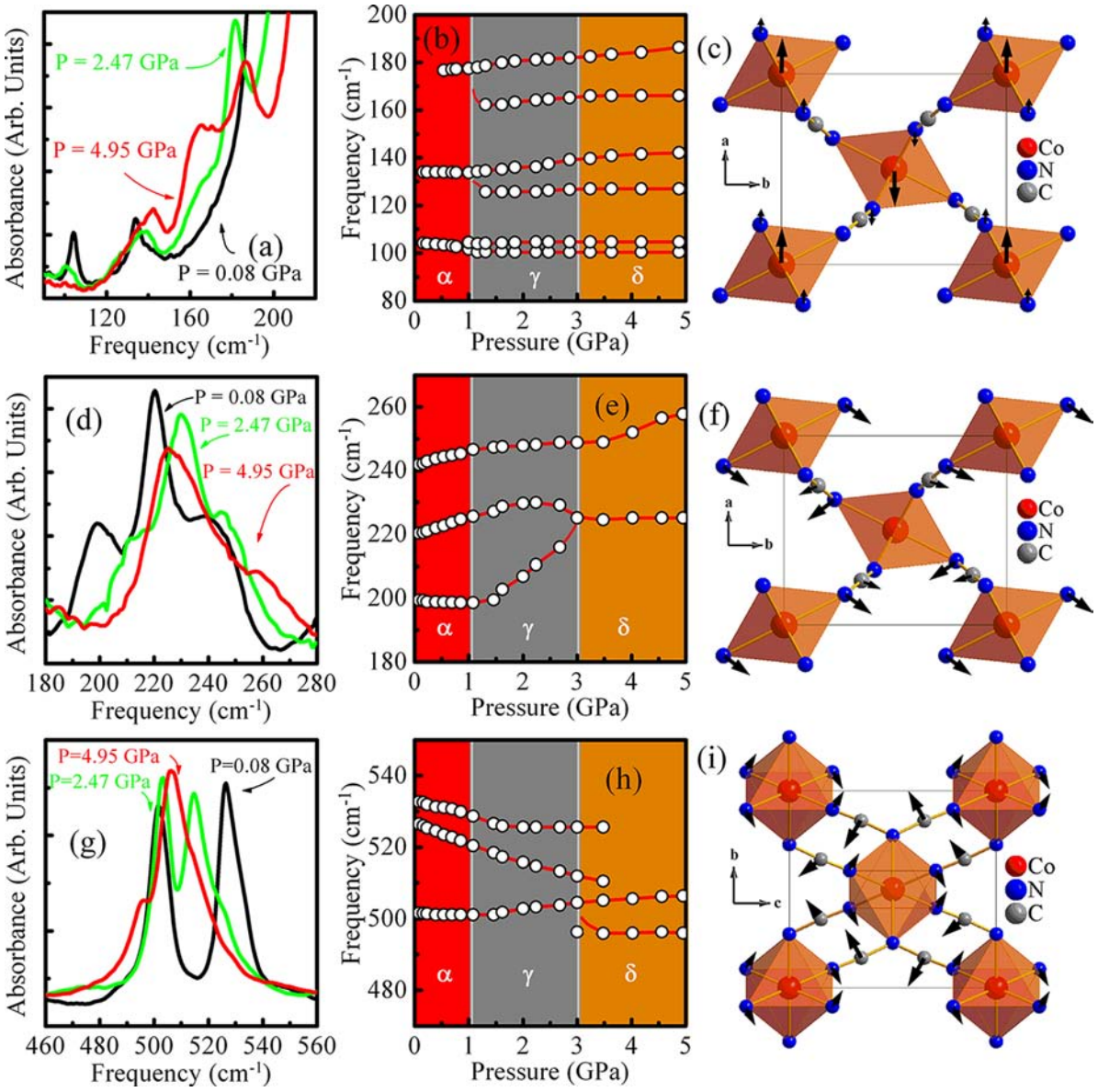

Figure 2. (a, d, g) Close-up views of the room temperature infrared response of α-$Co[N(CN)_2]_2$ at ambient pressure and ≈5 GPa. (b, e, h) Frequency vs pressure plots of this data. Error bars are less than the symbol size, and the thin solid lines guide the eye. Gray vertical lines denote critical pressures, and the three phases are labeled as α, γ, and δ. (c, f, i) Schematic diagrams of calculated displacement patterns for typical infrared-active modes in each range including the lattice mode involving Co^{2+} displacement along the *a*-axis (c), the N_{ax}—Co—N_{ax} bend (f), and the asymmetric N≡C—N deformation (δ_{as}(NCN)) (i).

symmetry and two Co^{2+} centers/cell.[39,40] Splitting of the low frequency lattice modes provides the strongest evidence for this conclusion. Infrared and Raman measurements reveal the transition to be somewhat sluggish, whereas it is sharp in early X-ray data.[26] Traditional length scale arguments, in which vibrational spectroscopies probe local structures at fast time scales and X-ray scattering probes the long-range average structure, reconcile these findings. As discussed below, the Raman spectra uncover a modest lattice component to the 3 GPa $\gamma \rightarrow \delta$ transition. Even so, it takes place within the context of a relatively similar crystal lattice and, as evidenced by the infrared response, involves additional ligand flexibility at higher pressure. Of course, crystallography probes long-range order and does not recognize a structural transition unless the space group changes. Spectroscopists take a broader view of this issue because there are many situations in which bulk structure and local symmetry investigations provide complementary information.[41,42] This perspective allows discovery of new regions in pressure−temperature−magnetic field space from which exotic properties may emerge.

Raman Scattering as a Probe of Pressure-Induced Lattice Distortions. Turning to the Raman response,[36] we again find rich pressure-driven changes in the spectrum. As before, the peaks are assigned based upon a symmetry analysis, dynamics calculations on the Mn analog, and comparison with chemically similar model compounds like $Na[N(CN)_2]$, $Co[C(CN)_3]_2$, and $K[C(CN)_3]$.[9] Figure 3 brings our findings together with close-up views of several interesting low frequency mode clusters, the associated frequency vs pressure trends, and schematic diagrams of representative calculated mode displacement patterns. That $Co[N(CN)_2]_2$ is a relatively

dx.doi.org/10.1021/ic402010h | *Inorg. Chem.* 2013, 52, 14148−14154

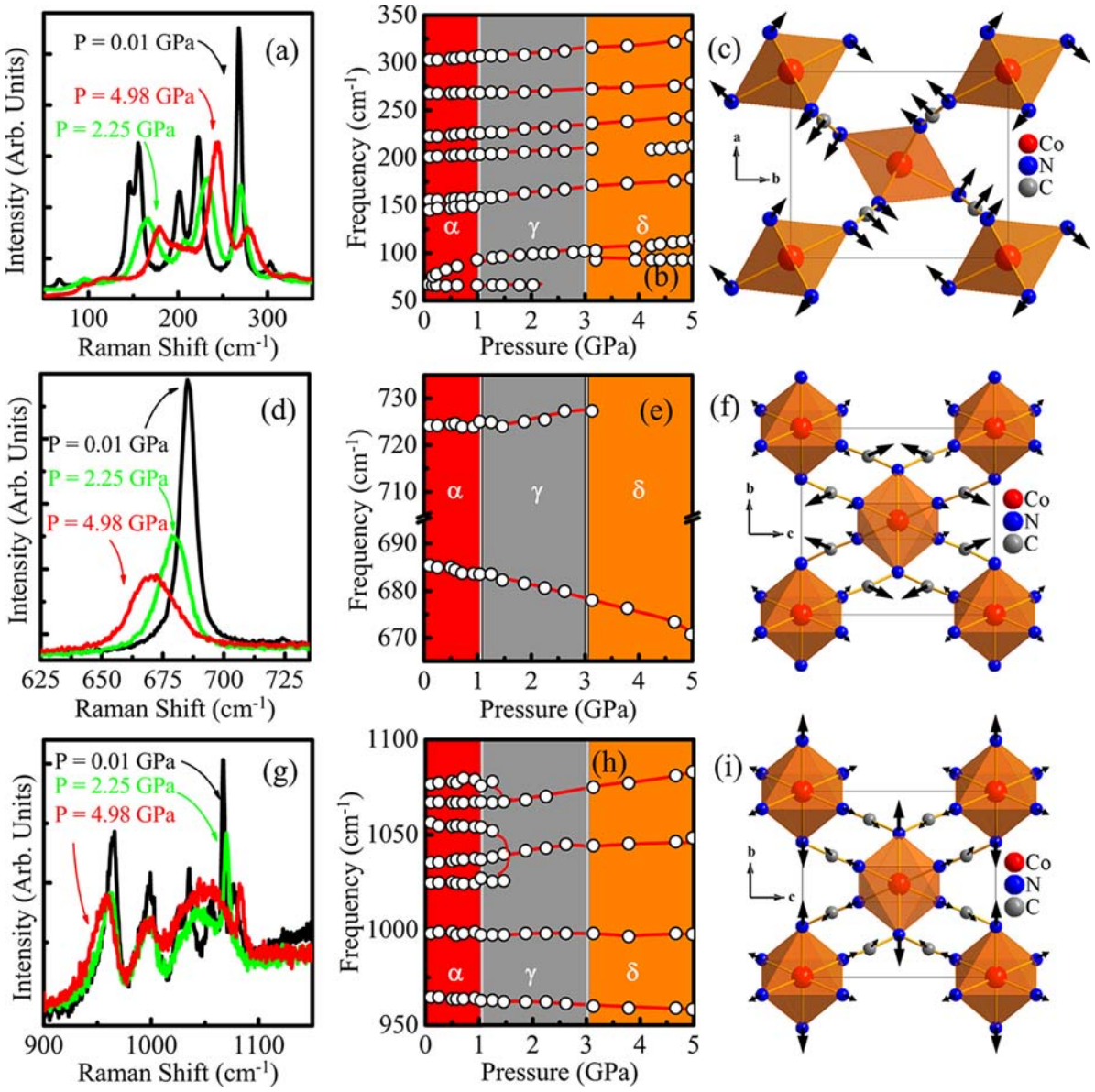

Figure 3. (a, d, g) Close up views of the room temperature Raman spectrum of α-$Co[N(CN)_2]_2$ at ambient pressure, 2.25 GPa, and ≈5 GPa. (b, e, h) Frequency vs pressure plots of this data. Error bars are less than the symbol size, and the thin solid lines guide the eye. Gray vertical lines denote critical pressures, and the three phases are labeled as α, γ, and δ. (c, f, i) Schematic diagrams of calculated displacement patterns for typical Raman-active modes in each range including the CoN_6 counter-rotation mode (c), the symmetric, in-phase, in-plane C—N—C bending mode (f), and the N—C stretching mode (i).

soft and flexible material is evident from the sensitivity of the Raman response to pressure.

One of the lowest frequency Raman-active vibrational modes is calculated to be a collective octahedral rotation about the *c*-axis (Figure 3c).[9,43] We assign the 67 cm^{-1} peak to this motion. It softens slightly with increasing pressure and hardens again before broadening through the $\alpha \rightarrow \gamma$ transition. Then it diminishes entirely. Relaxation of the counter-rotation mode is indicative of reduced strain under compression and a softer octahedral network. The latter is realized only when the CoN_6 building block units are successively antirotated.[44] Clearly, the displacement represented by the lowest frequency counter-rotation mode at 67 cm^{-1} does not provide an effective volume reduction pathway for α-$Co[N(CN)_2]_2$, at least not until the trend reverses above 0.7 GPa. Here, additional compression re-rotates the octahedra, and by 1 GPa, the overall trend is essentially neutral. Turning to the other component, the spectra reveal strong hardening of the higher frequency branch, which corresponds to concerted CoN_6 counter-rotation about the C_4 symmetry axes. This branch, which is theoretically predicted to be a doublet[9,43] but experimentally observed to be a singlet in the α- and γ-phases, is finally revealed as a doublet when degeneracy is relieved in the δ-phase. Splitting distinguishes CoN_6 rotations about *a* and *b*, consistent with Co^{2+} displacement mode symmetry breaking in the infrared (Figure 2a–c) and a true structural transition to a similar but slightly lower symmetry crystal group at 3 GPa. Although this structure blue-shifts over the full pressure range of investigation, hardening is especially pronounced in the α-phase where the peak moves from 76 to 93 cm^{-1} with $(\partial\omega/\partial P)_T$ = 15.4 cm^{-1}/GPa. That this set of counter-rotations stiffens is indicative of additional strain under compression. Successive counter-

dx.doi.org/10.1021/ic402010h | *Inorg. Chem.* 2013, 52, 14148–14154

rotations around the C_4 axis along with ligand compression offer an effective volume reduction pathway for α-Co[N-$(CN)_2]_2$. Similar octahedral counter-rotations accompany photomagnetic transitions in Prussian blue analogs and other transition metal cyanides.[45−47] They also contribute to the 30 T magnetic quantum critical transition in $Mn[N(CN)_2]_2$.[9]

Getting back to α-$Co[N(CN)_2]_2$, the spectra also reveal a 2 → 1 coalescence of the 150 cm^{-1} doublet at 1 GPa.[48] We assign the two components of this mode to Co—N_{ax}—$C_{(2)}$ and Co—$N_{eq(2)}$ wagging motions, respectively, and attribute the 1 GPa collapse of this structure to the $\alpha \rightarrow \gamma$ structural transition and crossover to a new crystal symmetry above 1 GPa.[49] We also find that the 685 cm^{-1} in-phase in-plane C—N_{ax}—C bend red-shifts 13.5 cm^{-1} (≈2%) over the pressure range of interest.[50] We extract $(\partial\omega/\partial P)_T$ = −2.7 cm^{-1}/GPa. The Raman-active C—N stretch at 965 cm^{-1} red-shifts as well. The increased line width may imply development of two different local C—N_{ax}—C environments (and unique superexchange pathways) under pressure. This supposition is consistent with the finding of pressure-induced distortion of the CoN_6 octahedra discussed in the prior section. Finally, the Raman-active C≡N stretch at 2215 cm^{-1} red-shifts by 13 cm^{-1} between 0 and 5 GPa, with most of the softening occurring through the $\alpha \rightarrow \gamma$ transition. There is typically an anticorrelation between the C≡N stretch and the bond length.[51]

How Do Local Structure Changes Contribute to the Magnetic Crossover? Local structure modifications are well-known to impact overlap integrals, superexchange interactions, and magnetic properties in a wide variety of materials.[27] As a result, there can be a strong positional dependence to the exchange interactions in a magnetic material.[53−57] Although the exact connection between these local lattice distortions and the pressure-induced ferromagnetic → antiferromagnetic crossover is still to be uncovered in α-$Co[N(CN)_2]_2$,[58] modified CoN_6 counter-rotations, distorted octahedra, and flatter C—N_{ax}—C linkages obviously impact the superexchange interactions and affect the magnetic state. For instance, the increased relative octahedral elongation under pressure makes $Co[N(CN)_2]_2$ more like the Mn analog,[38] which is antiferromagnetic. This type of spin−lattice interaction is of interest in a wide variety of compounds including Mn_3O_4, $ErNi_2B_2C$, $DyMn_2O_5$, and chlorocyclohexane.[11,15,17,59−73] For example, volume contraction drives high spin → low spin transitions in $[Ru_2(O_2CMe)_4]_3[Cr(CN)_6]$ and a number of spin crossover materials.[71,72] The pressure-dependent superexchange integral closely tracks T_N in CoO as well.[73]

Prospects for Negative Thermal Expansion in α-$Co[N(CN)_2]_2$. Like a number of other transition metal cyanides, α-$Co[N(CN)_2)]_2$ has several Raman- and infrared-active modes that red-shift with pressure. This behavior can be used to assess prospects for negative thermal expansion and negative linear compressibility.[74−77] Important shared physical characteristics include (i) a sparse crystal structure and (ii) transverse deformation phonons with negative mode Grüniessen parameters. The latter is defined as $\gamma_i = B_0(\partial \ln \omega_i/\partial P)$ and is a measure of each mode frequency's volume dependence. Here, B_0 is the bulk modulus (typically between 5 and 10 GPa[75]), and the ω_i's are the mode frequencies. All vibrational modes in a material contribute (with appropriate coefficients) to various thermodynamic response functions, although low energy mode contributions dominate.[78,79] Our spectra measurements and dynamics calculations reveal that octahedral rotation around c at 67 cm^{-1}, C—N—C and C—N ligand bending and stretching, and C≡N stretching at 2215 cm^{-1} soften with pressure.[80] Of these candidates, only the 67 cm^{-1} CoN_6 counter-rotation mode is likely to make an important contribution because, although the other features red-shift with pressure, they resonate at much higher frequencies. Closer examination of the 67 cm^{-1} counter-rotation mode reveals, however, that it red-shifts only slightly ($\partial\omega/\partial P$ = −1.2 cm^{-1}/GPa below 0.7 GPa) before flattening out and hardening again such that the frequency shift is close to neutral at 1 GPa. Because this mode does not go to zero or even soften significantly, it is unlikely that this system exhibits the desired characteristics, even in the 0−0.7 GPa regime.[81] The lack of very low frequency modes with strongly negative mode Grüneissen parameters bodes ill for the discovery of negative thermal expansion and/or negative linear compressibility in α-$Co[N(CN)_2)]_2$.

Pink → Blue Transition with Pressure? Finally, we return to the question of whether the β-phase of $Co[N(CN)_2]_2$ prepared by chemical means at ambient pressure is the same as that obtained from the α-phase under pressure. Figure 4 compares the infrared spectra of the two materials. Clearly, they are quite different, indicating that the as-synthesized ambient pressure form of β-$Co[N(CN)_2]_2$ does not have the same local structure as α-$Co[N(CN)_2]_2$ under the pressure conditions probed in these experiments. Moreover, the as-prepared β-phase material features Co^{2+} in a tetrahedral environment, which is blue.[18,22] Instead, quasi-isotropic pressure up to 5 GPa in the diamond anvil cell drives through phases that still appear pink, an observation that supports an octahedral Co^{2+}

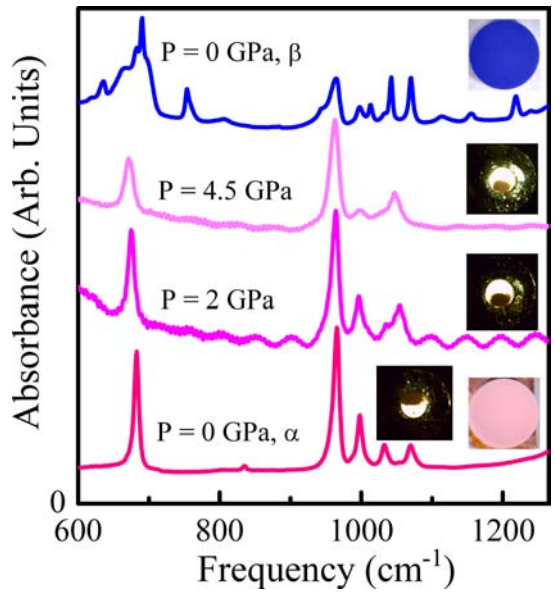

Figure 4. Comparison of a portion of the 300 K middle infrared spectrum of pink α-$Co[N(CN)_2]_2$ under various pressure conditions with the as-synthesized blue β-phase form under ambient conditions. Photographs of pressed powder samples show the pink and blue color, attributable to the octahedral vs tetrahedral transition metal environment in the two materials. The spectrum of β-$Co[N(CN)_2]_2$ does not match that found under the pressure conditions investigated here. Characteristic spectra, along with photos of the sample inside the diamond anvil cell, are presented for comparison. The images appear slightly different mostly because lighting is difficult to control. We detect only modest changes in the visible optics response in this pressure range.

dx.doi.org/10.1021/ic402010h | Inorg. Chem. 2013, 52, 14148−14154

coordination environment. The short-lived blue form does, however, appear at the edges of a KBr pellet when released from the die and when a sample of pink α-$Co[N(CN)_2]_2$ is pressed and sheared across a surface (for instance, between two microscope slides). We suspect that shear may play a role in these transitory processes,[25] although shearing in $[K_3Fe(CN)_6]$ (for instance) drives a change in oxidation state[82] rather than in the coordination environment of the transition metal center. It is worth pointing out that chemical transformations of the type that would have to take place to convert the pink (octahedral) form of $Co[N(CN)_2]_2$ into the blue (tetrahedral) form are usually not reversible, although there are exceptions.[83,84]

CONCLUSION

To summarize, there is broad and growing interest in the use of external stimuli to manipulate the properties of molecule-based materials. This work combines diamond anvil cell techniques with synchrotron-based infrared and Raman spectroscopy and complementary lattice dynamics calculations for a microscopic analysis of pressure-induced lattice distortions in α-$Co[N(CN)_2]_2$. We find that the $\alpha \rightarrow \gamma$ structural transition at 1 GPa takes place with a crystallographic change that doubles the number of Co^{2+} centers in the cell and reduces the symmetry. Local structure modifications include CoN_6 counter-rotation, distortion and relative elongation of the octahedra, and flattening of the $C—N_{ax}—C$ linkages. These distortions alter the superexchange interactions and may be related to the pressure-induced ferromagnetic → antiferromagnetic crossover. The phase transition at 3 GPa involves modest local lattice distortions within the context of a relatively similar space group. Our analysis of mode Grüniessen parameters reveals that this system is unlikely to display negative thermal expansion. Finally, we show that there is not a simple low pressure pathway between the pink α and blue β ambient pressure phases of $Co[N(CN)_2]_2$.

AUTHOR INFORMATION

Notes

The authors declare no competing financial interest.

ACKNOWLEDGMENTS

This research was supported by the PRF (52053-ND10, UT), NSF (DMR-1063880, UT and DMR-1005825, EWU), and the DoE (BNL, ANL). The U2A Beamline is supported by COMPRES under NSF Cooperative Agreement EAR 06-49658. We thank Y. Song for useful discussions and P. Chen for technical assistance.

REFERENCES

(1) Kahn, O. *Molecular magnetism*; VCH: New York, 1993.
(2) Callen, E.; Callen, H. B. *Phys. Rev.* **1965**, *139*, A455−A471.
(3) Bray, J. W.; Interrante, L. V.; Jacobs, I. S.; Bonner, J. *Extended linear chain compounds*; Miller, J. S., Ed.; Plenum: New York, 1983; Vol 3.
(4) Hase, M.; Terasaki, I.; Uchinokura, K. *Phys. Rev. Lett.* **1993**, *70*, 3651−3654.
(5) Sushkov, A. B.; Tchernyshyov, O.; Ratcliff, W., II; Cheong, S. W.; Drew, H. D. *Phys. Rev. Lett.* **2005**, *94*, 137202.
(6) Cheong, S. W.; Mostovoy, M. *Nat. Mater.* **2007**, *6*, 13−20.
(7) Lummen, T. T. A.; Chen, P.; Ramirez, M. O. ; Barnes, E. A.; Podraza, N. J.; Musfeldt, J. L.; Gopalan, V. Contributed Chapter for "Multiferroics", Ramesh, R., Martin, L. W., Eds.; Wiley: New York, in press.
(8) Musfeldt, J. L.; Vergara, L. I.; Brinzari, T. V.; Tung, L. C.; Wang, Y. J.; Schlueter, J. A.; Manson, J. L.; Sun, C.; Whangbo, M.-H. *Phys. Rev. Lett.* **2009**, *103*, 157401.
(9) Brinzari, T. V.; Chen, P.; Sun, Q.-C.; Liu, J.; Tung, L.-C.; Wang, Y.; Schlueter, J. A.; Singleton, J.; Manson, J. L.; Whangbo, M.-H.; Litvinchuk, A. P.; Musfeldt, J. L. *Phys. Rev. Lett.* **2013**, *110*, 237202.
(10) Halder, G. J.; Chapman, K. W.; Schlueter, J. A.; Manson, J. L. *Angew. Chem., Int. Ed.* **2011**, *50*, 419−421.
(11) Tian, P.; Zhang, Y.; Senevirathne, K.; Brock, S. L.; Dixit, A.; Lawes, G.; Billinge, S. J. L. *ACS Nano* **2011**, *5*, 2970−2978.
(12) du Trémolet de Lacheisserie, E.; Gignoux, D.; Schlenker, M. *Magnetism: fundamentals*; Springer Science: Boston, 2005.
(13) Zapf, V. S.; Correa, V. F.; Sengupta, P.; Batista, C. D.; Tsukamoto, M.; Kawashima, N.; Egan, P.; Pantea, C.; Migliori, A.; Betts, J. B.; Jaime, M.; Paduan-Filho, A. *Phys. Rev. B* **2008**, *77*, 020404(R).
(14) Chaudhury, R. P.; Lorenz, B.; Sun, Y. Y.; Bezmaternykh, L. N.; Temerov, V. L.; Chu, C. W. *Phys. Rev. B* **2010**, *81*, 220402(R).
(15) Vergara, L. I.; Cao, J.; Tung, L.-C.; Rogado, N.; Yen, F.; Wang, Y. Q.; Cava, R. J.; Lorenz, B.; Wang, Y.-J.; Musfeldt, J. L. *Phys. Rev. B* **2010**, *81*, 012403.
(16) Kim, M.; Chen, X. M.; Wang, X.; Nelson, C. S.; Budakian, R.; Abbamonte, P.; Cooper, S. L. *Phys. Rev. B* **2011**, *84*, 174424.
(17) Cao, J.; Vergara, L. I.; Musfeldt, J. L.; Litvinchuk, A. P.; Wang, Y. J.; Park, S.; Cheong, S.-W. *Phys. Rev. Lett.* **2008**, *100*, 177205.
(18) Manson, J. L.; Kmety, C. R.; Huang, Q.; Lynn, J. W.; Bendele, G. M.; Pagola, S.; Stephens, P. W.; Liable-Sands, L. M.; Rheingold, A. L; Epstein, A. J.; Miller, J. S. *Chem. Mater.* **1998**, *10*, 2552−2560.
(19) Kmety, C. R.; Manson, J. L.; Huang, Q.; Lynn, J. W.; Miller, J. S.; Epstein, A. J. *Phys. Rev. B* **1999**, *60*, 60.
(20) Nuttall, C. J.; Takenobu, T.; Iwasa, Y.; Kurmoo, M. *Mol. Cryst. Liq. Cryst. Sci. Technol., Sect. A* **2000**, *343*, 227−234.
(21) Lappas, A.; Wills, A. S.; Green, M. A.; Prassides, K.; Kurmoo, M. *Phys. Rev. B* **2003**, *67*, 144406.
(22) Kurmoo, M.; Kepert, C. J. *New J. Chem.* **1998**, *22*, 1515−1524.
(23) Kmety, C. R.; Manson, J. L.; McCall, S.; Crow, J. E.; Stevenson, K. L.; Epstein, A. J. *J. Magn. Magn. Mater.* **2002**, *248*, 52−61.
(24) In our work, we employ a "single J" Hamiltonian of the form $\mathcal{H} = -(1/2)\sum_{i\neq j}J_{ij}\mathbf{S}_i\cdot\mathbf{S}_j - D\sum_i \mathbf{S}_{iz}^2 - g\mu_B B\sum_i \mathbf{S}_{iz}$, where J = 4 K is the exchange interaction,[23] $D = 12 \pm 4$ cm^{-1} is the anisotropy energy,[43] g = 5.34 is the electron g-factor, $\mathbf{S}_i$ is the local moment on site i, and B is the external magnetic field.
(25) The blue color on the sides of a KBr pellet is short-lived and lasts for only a few seconds or at most a minute after release of the pellet from the die, and it appears only around the edges (where there may be additional shearing forces).
(26) Halder, G. J. Unpublished work.
(27) Goodenough, J. *Magnetism and the chemical bond*; Wiley: New York, 1963.
(28) Mao, H. K.; Xu, J.; Bell, P. M. *J. Geophys. Res., [Solid Earth Planets]* **1986**, *91*, 4673−4676.
(29) Carr, G. L.; Martin, M. C.; McKinney, W. R.; Neil, G. R.; Jordan, K.; Williams, G. P. *Nature* **2002**, *420*, 153−156.
(30) Hammer, B.; Hansen, L. B.; Norskov, J. K. *Phys. Rev. B* **1999**, *59*, 7413.
(31) Clark, S. J.; Segall, M. D.; Pickard, C. J.; Hasnip, P. J.; Probert, M. I. J.; Refson, K.; Payne, M. C. *Z. Kristallogr.* **2005**, *220*, 567−570.
(32) Monkhorst, H. J.; Pack, J. D *Phys. Rev. B* **1976**, *13*, 5188.
(33) Refson, K.; Clark, S. J.; Tulip, P. R. *Phys. Rev. B* **2006**, *73*, 155114.
(34) Musfeldt, J. L.; Kamarás, K.; Tanner, D. B. *Phys. Rev. B.* **1992**, *45*, 10197.
(35) Fateley, W. G.; Dollish, F. R.; McDevitt, N. T.; Bentley, F. F. *Infrared and Raman selection rules for molecular and lattice vibrations: the correlation method*; Wiley-Interscience: New York, 1972.
(36) Although all of the infrared-active modes (and some of their overtones and combinations) are accounted for, only about half of the predicted Raman-active modes are present in the spectrum. This makes assignment of the low frequency Raman modes a challenge,

even with the benefit of complementary dynamics calculations. Raman scattering is also sensitive to electronic and magnetic excitations.[43,73] We do not see evidence for these features here, mainly due to the weak field dicyanamide ligands (compared to CoO, for instance[73]), which lower the overall energy scale.
(37) These modes soften with decreasing temperature.[43]
(38) Kmety, C. R.; Huang, Q.; Lynn, J. W.; Erwin, R. W.; Manson, J. L.; McCall, S.; Crow, J. E.; Stevenson, K. L.; Miller, J. S.; Epstein, A. J. *Phys. Rev. B* **2000**, *62*, 5576.
(39) A new set of normal modes characterize each phase.
(40) The ambient phase atom−atom connectivity is maintained over the entire pressure range of our investigation.
(41) Chen, M.; Tanner, D. B.; Nino, J. C. *Phys. Rev. B* **2005**, *72*, 054303.
(42) K., H.; Stephens, P. W.; Martin, C.; Constable, E.; Lewis, R. A.; Berger, H.; Carr, G. L.; Tanner, D. B. *Phys. Rev. B* **2012**, *86*, 174104.
(43) Brinzari, T. V.; Haraldsen, J. T.; Chen, P.; Sun, Q.-C.; Kim, Y.; Tung, L.-C.; Schlueter, J. A.; Wang, Y. J.; Smirnov, D.; Manson, J. L; Singleton, J.; Musfeldt, J. L. *Phys. Rev. Lett.* **2013**, *111*, 047202.
(44) The CoN_6 octahedra successively antirotate with decreasing temperature as well.[38]
(45) Sato, O.; Iyoda, T.; Fujishima, A.; Hashimoto, K. *Science* **1996**, *272*, 704−705.
(46) Zentková, M.; Arnold, Z.; Kamarád, J.; Kavecanský, V.; Lukácova, M.; Mat'as, S.; Mihalik, M.; Mitróová, Z.; Zentko, A. *J. Phys.: Condens. Matter* **2007**, *19*, 266217.
(47) Pajerowski, D. M.; Gardner, J. E.; Frye, F. A.; Andrus, M. J.; Dumont, M. F.; Knowles, E. S.; Meisel, M. W.; Talham, D. R. *Chem. Mater.* **2011**, *23*, 3045−3053.
(48) Several other features display these trends as well.
(49) The splitting of these bending modes collapses with pressure, widens with decreasing temperature, and red-shifts by 0.5 cm^{-1} with magnetic field.
(50) This mode is variously described in the literature as a symmetric, in-phase, in-plane C—N—C bend or as a symmetric, in-phase, in-plane N—C≡N bend. The displacement pattern contains mostly C motion. The former classification seems more revealing because it regards motion in terms of the whole dicyanamide ligand rather than just the N—C—N fragment.
(51) This is because the CN is both a σ-donor (which tends to raise the frequency) and a π-acceptor (which tends to soften the frequency due to back-bonding and other effects.[52,70,76,77]
(52) Cremer, D.; Wu, A.; Larsson, A.; Kraka, E. *J. Mol. Model.* **2000**, *6*, 396−412.
(53) Anderson, P. W. *Solid State Physics*; Academic Press: New York and London, 1963; Vol. *14*, p 99.
(54) Whangbo, M.-H.; Koo, H. J.; Dai, D. *J. Solid State Chem.* **2003**, *176*, 417.
(55) Baltensperger, W. *J. Appl. Phys.* **1970**, *41*, 1052−1054.
(56) Fennie, C. F.; Rabe, K. R. *Phys. Rev. Lett.* **2006**, *96*, 205505.
(57) Similar mechanisms have been invoked to explain high magnetic field effects in $Mn[N(CN)_2]_2$ and other molecule-based materials.[8,9]
(58) In situ pressure and temperature spectroscopy will probe this connection.
(59) Rho, H.; Klein, M. V.; Canfield, P. C. *Phys. Rev. B* **2004**, *69*, 144420.
(60) Gupta, R.; Kim, M.; Barath, H.; Cooper, S. L.; Cao, G. *Phys. Rev. Lett.* **2006**, *96*, 067004.
(61) Dong, Z.; Beulby, N. G.; Huang, Y.; Song, Y. *J. Chem. Phys.* **2008**, *128*, 074501.
(62) de la Cruz, C. R.; Yen, F.; Lorenz, B.; Park, S.; Cheong, S.-W.; Gospodinov, M. M.; Ratcliff, W.; Lynn, J. W.; Chu, C. W. *J. Appl. Phys.* **2006**, *99*, 08R103.
(63) Song, Y.; Murli, C.; Liu, Z. *J. Chem. Phys.* **2009**, *131*, 174506.
(64) Imai, T.; Ahilan, K.; Ning, F. L.; McQueen, T. M.; Cava, R. J. *Phys. Rev. Lett.* **2005**, *102*, 177005.
(65) Kim, M.; Chen, X. M.; Joe, Y. I.; Fradkin, E.; Abbamonte, P.; Cooper, S. L. *Phys. Rev. Lett.* **2010**, *104*, 136402.
(66) Sun, Q. C.; Baker, S. N.; Christianson, A. D.; Musfeldt, J. L. *Phys. Rev. B* **2011**, *84*, 014301.
(67) Shinaoka, H.; Tomita, Y.; Motome, Y. *Phys. Rev. Lett.* **2011**, *107*, 047204.
(68) Ramazanoglu, M.; Ratcliff, W., II; Yi, H. T.; Sirenko, A. A.; Cheong, S.-W.; Kiryukhin, V. *Phys. Rev. Lett.* **2011**, *107*, 067203.
(69) Walker, H. C.; Fabrizi, F.; Paolasini, L.; de Bergevin, F.; Herrero-Martin, J.; Boothroyd, A. T.; Prabhakaran, D.; McMorrow, D. F. *Science* **2011**, *333*, 1273−1276.
(70) Brinzari, T. V.; Chen, P.; Tung, L.-C.; Kim, Y.; Smirnov, D.; Singleton, J.; Miller, J. S.; Musfeldt, J. L. *Phys. Rev. B* **2012**, *86*, 214411.
(71) Fishman, R. S.; Shum, W. W.; Miller, J. S. *Phys. Rev. B* **2010**, *81*, 172407.
(72) Hauser, A. *Top. Curr. Chem.* **2004**, *234*, 155−198.
(73) Struzhkin, C. C.; Goncharov, A. F.; Syassen, K. *Mater. Sci. Eng.* **1993**, *A168*, 107−110.
(74) Chapman, K. W.; Chupas, P. *J. Am. Chem. Soc.* **2007**, *129*, 10090−10091.
(75) Goodwin, A. L.; Keen, D. A.; Tucker, M. G. *Proc. Natl. Acad. Sci. U. S. A.* **2008**, *105*, 18708−18713.
(76) Romao, C.; Barsan, M. M.; Butler, I. S.; Gilson, D. F. R. *J. Mater. Sci.* **2010**, *45*, 2518−2520.
(77) Barsan, M. M.; Butler, I. S.; Pitzpatrick, J.; Gilson, D. F. R. *J. Raman. Spectrosc.* **2010**, *42*, 1820−1824.
(78) This is because these modes are most easily populated with temperature and most easily deformed under pressure, tendencies that give large positive (or large negative) elastic compliances.
(79) This emphasis on low frequency mode contribution is exemplified by the coefficient of thermal expansion $\alpha = \sum_i \alpha_i = (C_T/V)\sum_i S_{ji}\gamma_i$, where C_T is the isothermal specific heat, V is the unit cell volume, and the S_{ji} are elastic compliances.
(80) The character of many of these modes is deformation-like with displacement patterns that allows the ligands to buckle, and as already indicated, they either counter-rotate the CoN_6 octahedra or control the magnetic interactions between the Co^{2+} centers (that reside in the stiffer CoN_6 octahedra).
(81) In addition to summing over the vibrational modes, the compliance coefficients can take on either positive or negative values.
(82) Lewis, G. J.; Whalley, E. *J. Chem. Phys.* **1967**, *47*, 2591−2294.
(83) Song, Y.; Murli, C.; Liu, Z. *J. Chem. Phys.* **2009**, *131*, 174506.
(84) Murli, C.; Song, Y. *J. Phys. Chem. B* **2009**, *113*, 13509−13515.